Nanoscale

PAPER

View Article Online
View Journal | View Issue

Cite this: *Nanoscale*, 2014, **6**, 1573

Gold nanoparticle-decorated graphene oxides for plasmonic-enhanced polymer photovoltaic devices†

Ming-Kai Chuang,[a] Shih-Wei Lin,[a] Fang-Chung Chen,*[a] Chih-Wei Chu[b] and Chain-Shu Hsu[c]

Received 23rd September 2013
Accepted 14th November 2013

DOI: 10.1039/c3nr05077g

www.rsc.org/nanoscale

In this work, gold nanoparticle/graphene oxide (AuNP/GO) nanocomposites are synthesized and used as anodic buffer layers in organic photovoltaic devices (OPVs). The application of thiol-terminated polyethylene glycol as a capping agent prevents the aggregation of AuNPs on the GO surface and further improves the solubility and stability of these nanomaterials in solutions. When AuNP/GO nanomaterials served as the buffer layers, they introduced localized surface plasmon resonance (LSPR) in the OPVs, leading to noticeable enhancements in the photocurrent and the efficiencies of the OPVs. We attribute the primary origin of the improvement in device performance to local field enhancement induced by the LSPR. We anticipate that this study might open up new avenues for constructing plasmon-enhancing layers on the nanoscale to improve the performance of solar cells.

Introduction

Organic photovoltaic devices (OPVs) incorporating bulk heterojunctions are attractive systems for harvesting solar energy because of their lightweight and mechanical flexibility and for their ease of preparation in large-area panels at low cost.[1–4] Moreover, the energy pay-back time—the length of time required for an energy-producing system or device to generate as much energy as that required for its manufacture—of an OPV can be amazingly short (on the order of several weeks) because its fabrication can be performed at low temperature, unlike the processes employed to prepare photovoltaic cells based on silicon or other inorganic materials.[5] Recently, OPVs with power conversion efficiencies (PCEs) of up to approximately 10% have been obtained through the development of novel materials having low band gaps and novel device structures.[6] Further improvements in the efficiency and reliability will, however, be required if these OPVs are to compete with inorganic solar technologies.

The internal quantum efficiencies of state-of-art OPVs are approaching close to 100%.[7] Their photoactive layers are usually thin, typically on the order of 100 nm, so that they can perform high-efficiency charge collection while minimizing the degree of charge recombination, but, thereby resulting in incomplete absorption of the incident solar irradiation. The use of films that are too thick will inevitably decrease the charge collection efficiency, due to the low carrier motilities of organic materials. Therefore, the challenge remains to achieve OPVs with high absorption efficiencies when using a thin photoactive layer. To solve this problem, many approaches for trapping light have been proposed to improve the absorption efficiency without affecting the charge collection efficiency,[8–17] for example, using folded device architectures to increase the optical length[8,9] or incorporating optical spacers to redistribute the optical electrical field, thereby effectively improving the light harvesting efficiency.[10,11] Among the techniques developed for trapping light, exploiting the surface plasmon resonance effect of metal nanostructures has been proved to be an effective strategy.[12–16] For example, metal nanoparticles (NPs) that can trigger localized surface plasmon resonance (LSPR) have been introduced into OPVs to enhance their light-trapping ability; incorporating such metal NPs in either the photoactive layers[13,14] or their vicinity[15–18] can improve device efficiencies. To simplify device fabrication, metal NPs are frequently blended with device buffer layers—for example, poly(3,4-ethylenedioxythiophene):polystyrenesulfonate (PEDOT:PSS); although such simple structures have been used widely, PEDOT:PSS itself has highly acidic and hygroscopic properties, leading to poor long-term stability.[19]

Graphene oxide (GO), the oxidized form of graphene, consists of a two-dimensional nanosheet derivatized chemically with oxygen-containing functional groups (*e.g.*, carbonyl, hydroxyl, and epoxide units).[20–23] GO can be prepared readily through chemical exfoliation from oxide graphite after ultrasonication, with the products being well dispersed in water.

[a]*Department of Photonics and Display Institute, National Chiao Tung University, Hsinchu 30010, Taiwan. E-mail: fcchen@mail.nctu.edu.tw*

[b]*Research Center for Applied Sciences, Academic Sinica, Taipei, 11529, Taiwan*

[c]*Department of Applied Chemistry, National Chiao Tung University, Hsinchu 30010, Taiwan*

† Electronic supplementary information (ESI) available. See DOI: 10.1039/c3nr05077g

Because GO is solution-processable, thermal or chemical reduction of GO is considered to be a promising approach for the preparation of graphene sheets in large quantities.[20,23] Recently, GO and reduced GO (rGO) have been reported as effective interlayers when positioned between the electrodes and the photoactive layer in OPVs.[24–29] For example, Li *et al.* reported the improved efficiencies of OPVs when employing solution-processable GOs as an alternative to PEDOT:PSS in the hole transport layer (HTL);[25] they found that the GO effectively suppressed the leakage current and lowered the rate of hole–electron recombination. In 2011, Yun *et al.* used the reduced form of GO to prepare a device having a greater stability than that of the corresponding device incorporating PEDOT:PSS.[26]

The presence of oxygen functionalities on the surface of GO provides reactive sites for chemical modification.[21] Therefore, GO can be considered as a promising nanoscale building block, having an ultrahigh surface area, for the preparation of novel composites featuring specific functionalities. Herein, we report the synthesis and characterization of gold nanoparticle/graphene oxide (AuNP/GO) nanocomposites for triggering LSPRs in polymer solar cells. We have found that the morphology of the AuNPs on the GO surface can be manipulated by controlling the amount of the capping agent for the NPs added during their synthesis. More importantly, these AuNP/GO nanocomposites can function effectively as anodic buffer layers in OPVs, providing observable enhancements in the photocurrent and overall device efficiency.

Results and discussion

Scheme 1 presents the synthesis of the AuNP/GO nanocomposites.[30,31] First, a mixture of an aqueous GO solution and a $HAuCl_4$ solution was heated at 80 °C; a reducing agent, sodium citrate, was added and then the mixture was maintained at 80 °C for 4 h while stirring continuously. After cooling the resulting solution to room temperature, thiol-terminated poly(ethylene glycol) (PEG–SH) was added to the solution to modify the surfaces of the AuNPs. After stirring for 1 h, the solution was centrifuged and washed with DI water. The resulting AuNP/GO composites were dried through lyophilization. Fig. 1 and S1† display transmission electron microscopy (TEM) images of AuNP/GO samples prepared with various amounts of PEG–SH. For all the samples, the AuNPs anchored on the GO surfaces were nearly spherical and highly uniform in size; the average size of the AuNPs attached to the GOs was approximately 18 nm. High-resolution images of the samples (Fig. S2†) confirmed the shapes and sizes of these NPs on the GO surfaces. Because the sizes of the AuNPs were almost identical, we suspect that the NP size was determined during the first step of sodium citrate-mediated reduction of the Au ions. The nucleation and growth of these NPs were complete prior to the addition of PEG–SH, which functioned merely to exchange the weakly capped citrate ions on the surface of the AuNPs. Many previous studies have indicated that the oxygen functionalities on GO surfaces behave as nucleation sites for AuNPs.[30–32] In this present investigation, we found that, in addition to individual AuNPs anchoring on the GO surfaces, many free-standing NPs originally produced in solution aggregated with those attached to the GO surface. After the addition of PEG–SH, the presence of this capping agent prevented further aggregation of the AuNPs. The NPs that were not bound directly to the GO surfaces were easier to remove during the washing step.

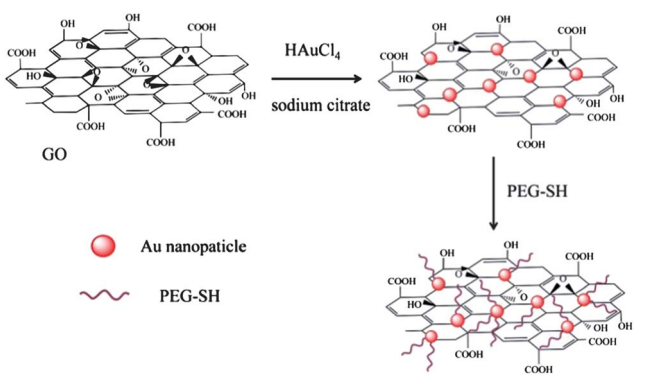

Scheme 1 Synthesis of AuNP/GO composites.

In addition to differences in morphology, the solutions of AuNP/GO nanocomposites modified with PEG–SH exhibited better stability. Fig. 2a presents the results of solubility tests of the AuNP/GO nanocomposites. Although all of the nanocomposites could be dispersed well in water after sonication, we occasionally observed small amounts of black powders in solutions of the AuNP/GO nanocomposite prepared without PEG–SH after aging for 15 days. After 40 days, however, precipitates began to appear. In contrast, the solutions containing the PEG–SH-modified AuNP/GO composites remained stable even after aging for 40 days, suggesting their higher solubility.

We used UV-Vis absorption to further characterize the AuNP/GO nanocomposites. As revealed in Fig. 2b, an aqueous solution of GO exhibited typical absorption peaks at 230 and 305 nm, corresponding to π–π* transitions of the C=C bonds and n–π* transitions of the carbonyl groups, respectively.[33] Upon reduction with sodium citrate, the spectra of the AuNP/GO nanocomposites retained these two characteristic absorptions with no shifts in their positions, suggesting that any changes in the GO structures were insignificant. Meanwhile, we observed absorption signals near 540 nm, indicating the formation of AuNPs on the GOs.

Raman spectroscopy is a highly effective tool for probing the structural changes of carbon materials.[34,35] Fig. 3 displays the Raman spectra of our AuNP/GO nanocomposites. Each spectrum exhibits two characteristic peaks: a D band (*ca.* 1314 cm^{-1}) corresponding to the breathing mode of κ-point phonons of A_{1g} symmetry and a G band (*ca.* 1600 cm^{-1}) arising from first-order scattering of the E_{2g} phonon of sp^2-hybridized C atoms.[30] The D band could also originate from bonds between sp^3-hybridized atoms, formed through oxidation, and other defects, such as vacancies, grain boundaries, and disordered carbon structures.[34] The ratio of the intensities of the D and G bands (I_D/I_G) is often used as a parameter for estimating the in-plane sp^2 domain size of a graphene structure.[33] The I_D/I_G ratio of the GO

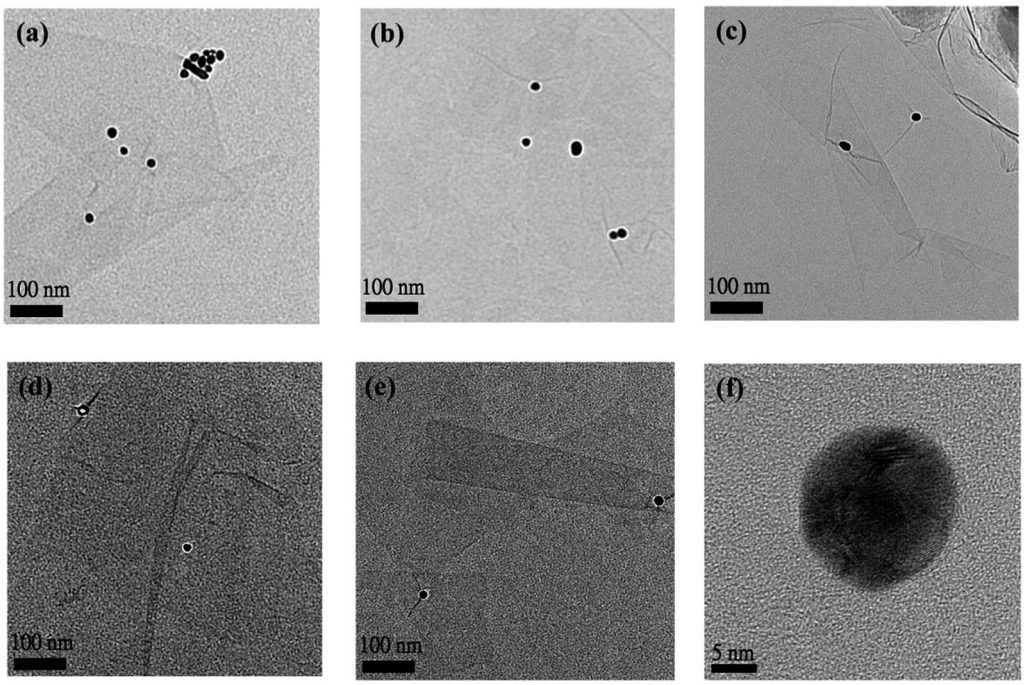

Fig. 1 (a–e) TEM images of AuNP/GO nanocomposites prepared at concentrations of PEG–SH of (a) 0, (b) 0.07, (c) 0.13, (d) 0.26, and (e) 0.52 mM. (f) High-resolution image of a typical AuNP; the PEG–SH concentration was 0.26 mM.

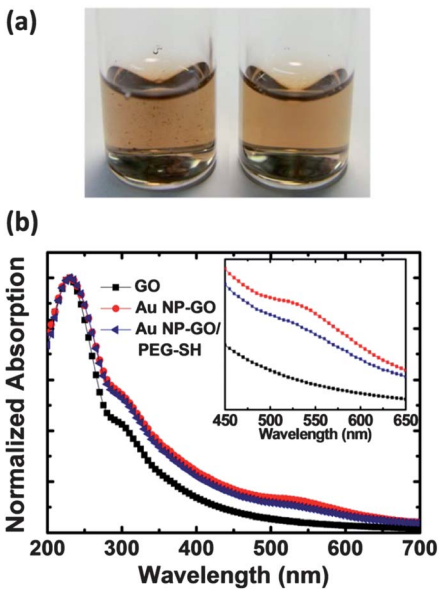

Fig. 2 Physical properties and characteristics of AuNP/GO nanocomposites. (a) Photograph of an aqueous dispersion of the AuNP/GO nanocomposites prepared (right) with and (left) without PEG–SH after aging for 40 days. A precipitate is evident in the left-hand bottom. (b) UV-Vis absorption spectra of GO and AuNP/GO nanocomposites in water; inset: spectra in the range 450–650 nm.

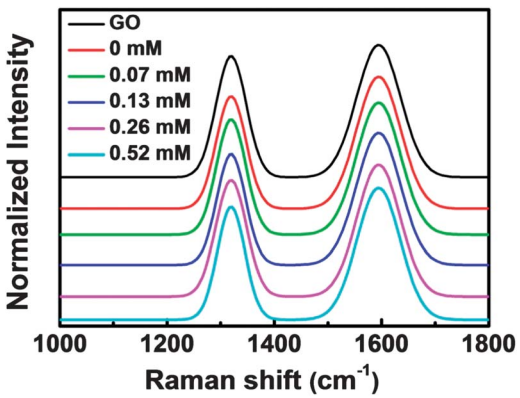

Fig. 3 Raman spectra of GO and the nanocomposites prepared under different conditions.

was 0.99; it reached approximately 0.90 after the reduction reactions. Table 1 summarizes the I_D/I_G ratios. Because the change in the intensity ratio was less than 10%, the Raman spectra indicated that our GOs were reduced only slightly by sodium citrate under the synthesis conditions we applied in this study. These results are consistent with the UV-Vis spectroscopic absorption data.

Fig. 4a displays the device structure incorporating the GO composites and the current density–voltage (J–V) characteristics

Table 1 Peak intensity ratios I_D/I_G of AuNP/GO materials prepared under various conditions

Sample (PEG–SH concentration, mM)	I_D/I_G ratio
GO	0.99
AuNP/GO (0)	0.90
AuNP/GO (0.07)	0.90
AuNP/GO (0.13)	0.89
AuNP/GO (0.26)	0.91
AuNP/GO (0.52)	0.91

of the OPVs obtained under illumination with simulated solar light (AM 1.5G). The device prepared with neat GOs as the HTL exhibited a value of V_{oc} of 0.57 V, a short-circuit current density (J_{sc}) of 8.87 mA cm^{-2}, and a fill factor (FF) of 0.65, resulting in a PCE of 3.26%. For the devices incorporating AuNP/GO composites, we observed that the direct use of the as-synthesized AuNP/GO composites resulted in very poor device performance, probably because of a very strong back-scattering by the AuNPs. Therefore, we further blended the solution with neat GOs to reduce the amount of AuNPs in the devices. The concentrations of AuNP/GO and GO were adjusted to 0.110 and 0.165 mg mL^{-1}, respectively. After decoration of the AuNPs on the GO surface, the value of V_{oc} decreased to 0.55 V, suggesting that the anodic interface was affected. Although the value of J_{sc} increased to 9.37 mA cm^{-2}, the FF also decreased slightly to 0.62 (Table 2); as a result, the PCE was 3.25%. As mentioned above, the AuNP/GO nanocomposites prepared without PEG–SH exhibited lower solubility and stability in solution, possibly resulting in rather poor quality thin films when deposited on the ITO surface. Therefore, we could not observe significant device enhancement.

For the device prepared using the PEG–SH-modified nanocomposites, however, the value of V_{oc} remained unchanged at 0.57 V, suggesting that the anodic interface was not significantly affected. The value of J_{sc} and the FF both improved to 10.44 mA cm^{-2} and 0.67, respectively, resulting in an increase in the PCE to 3.98%. Note, however, that the concentration of AuNPs in the buffer layer also had to be tuned properly with neat GOs (Fig. S3†). This performance suggests that the PEG–SH-modified AuNP/GO nanocomposites introduced their plasmonic

Table 2 Electrical characteristics of devices fabricated with GO and various AuNP/GO nanocomposites as anode buffer layers

Device condition (PEG–SH concentration, mM)	V_{oc} (V)	J_{sc} (mA cm^{-2})	FF (%)	PCE (%)
Neat GO[a]	0.57	8.87	64.5	3.26
AuNP/GO (0)[a]	0.55	9.37	63.0	3.25
AuNP/GO (0.07)[a]	0.57	9.63	64.9	3.56
AuNP/GO (0.13)[a]	0.57	10.44	66.8	3.98
AuNP/GO (0.26)[a]	0.57	10.04	66.9	3.83
AuNP/GO (0.52)[a]	0.57	9.95	66.7	3.78
Neat GO[b]	0.81	8.61	57.7	4.02
AuNP/GO (0.13)[b]	0.81	9.94	62.7	5.05

[a] Photoactive materials were P3HT and PCBM. [b] Photoactive materials were P3HT and ICBA.

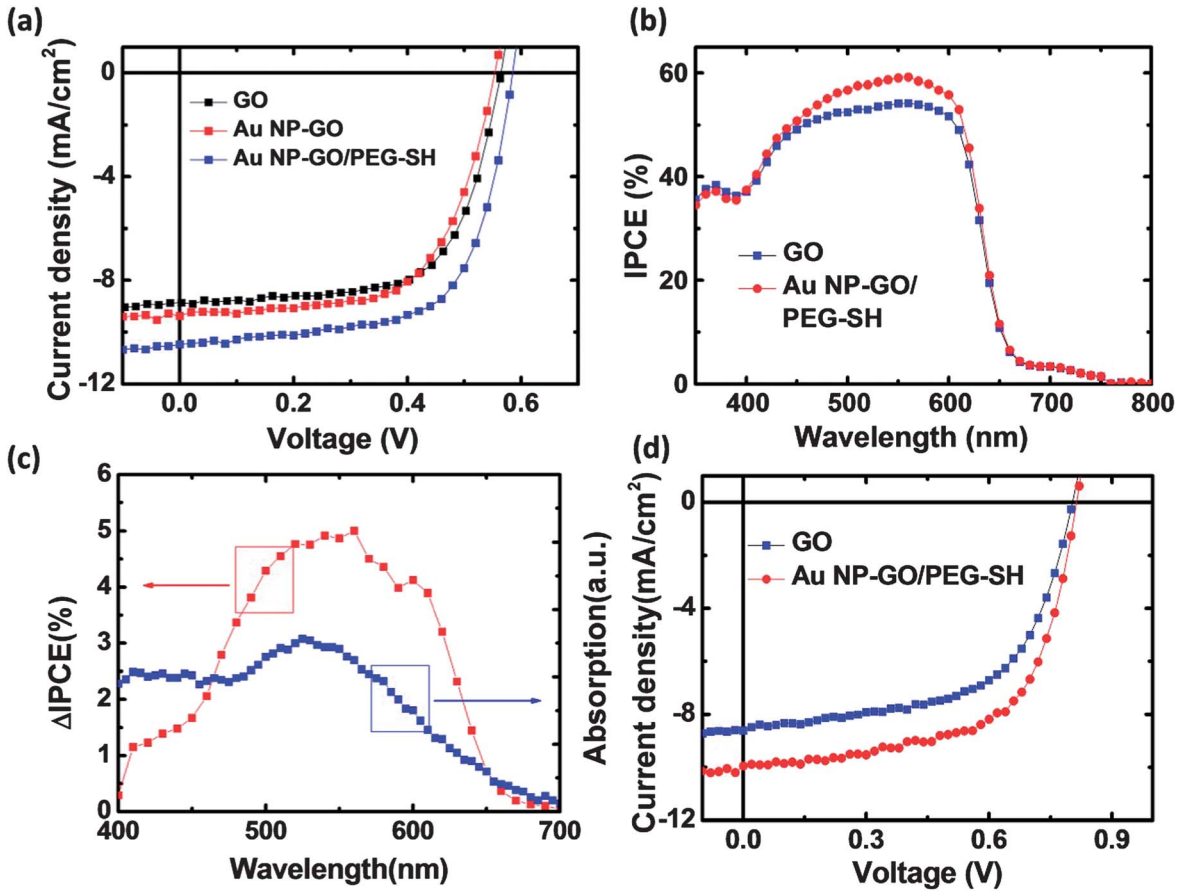

Fig. 4 (a) Current density–voltage (J–V) curves of devices prepared with various types of AuNP/GO composites as the anode buffer layer, under illumination at 100 mW cm^{-1} (AM 1.5G). (b) IPCE curves of OPV devices fabricated with GO and the PEG–SH-modified AuNP/GO composite. (c) The curve of the difference in IPCE (ΔIPCE) after using the AuNP/GO anode buffer layer compared with the absorption spectrum of the PEG–SH-modified AuNP/GO composite. (d) J–V curves of OPV devices prepared with P3HT:ICBA blends, recorded under illumination.

effect without affecting the electrical properties. Furthermore, we observed that the amount of PEG–SH used during the synthesis process affected the device performance. Fig. S4† displays the effect of the amount of PEG–SH on the *J*–*V* characteristics of OPVs incorporating the AuNP/GO nanocomposites. We observe that the device performance, especially the photocurrent, improved through the use of PEG–SH. The optimal device was that constructed when the concentration of PEG–SH during the second synthesis step was 0.13 mM; a further increase in the amount of PEG–SH resulted in a decrease in the value of J_{sc}. Because we could not observe any significant differences in morphology among the corresponding TEM images, we infer that the excess of PEG–SH blocked the transportation of holes and decreased the charge collection efficiency.

To further investigate the LSPR effect, we measured the incident photon-to-electron conversion efficiencies (IPCEs) of the various devices; Fig. 4b displays the results. The photocurrent increased after incorporating the AuNPs. Comparing the curve of the increase in IPCE (ΔIPCE) with the extinction spectrum of the AuNP/GO nanocomposite (Fig. 4c), we observe that the wavelength regime in which the photocurrent increased coincides with the extinction range of the AuNPs, indicating that excitation of the LSPR was responsible for the improved efficiencies.[15] Note that the absorption spectrum of the PEG–SH-modified AuNP/GO composite was obtained by subtracting the absorption of GO from that of AuNP/GO nanocomposites, which should reflect the real plasmonic behavior of the nanocomposites.

To explore the potential plasmonic effects of our PEG–SH-modified AuNP/GO nanocomposites for OPV applications, we further employed other photoactive materials to build photovoltaic devices. For example, the device V_{oc} has been found to be linked to the energy difference between the lowest unoccupied molecular orbital (LUMO) of the electron acceptor and the highest occupied molecular orbital (HOMO) of the electron donor in the polymer blends.[36,37] Therefore, indene–C_{60} bisadduct (ICBA) has a higher-energy LUMO than that of PCBM and can increase values of V_{oc} and PCEs.[36,37] Fig. 4d displays the *J*–*V* curves of devices fabricated with P3HT:ICBA blends, obtained under standard AM 1.5G illumination conditions. We observed similar improvements in device performance after using the PEG–SH-modified AuNP/GO nanocomposite as the HTL. The solar cell incorporating the GOs exhibited a value of V_{oc} of 0.81 V, a value of J_{sc} of 8.61 mA cm^{-2}, and an FF of 0.58, yielding a PCE of 4.02%. As expected, after decoration of the GO with AuNPs, the value of J_{sc} and the FF both improved to 9.94 mA cm^{-2} and 0.63, respectively, while the value of V_{oc} remained unchanged, thereby increasing the PCE to 5.05%. The IPCE spectra also revealed a similar trend for the photocurrent (Fig. S5†). These results suggest that PEG–SH-modified AuNP/GO nanocomposites have great potential for OPV applications.

Previously, we blended AuNPs into PEDOT:PSS HTLs to improve device efficiencies;[15] we attributed these improvements in device performance to plasmonic effects. To confirm these effects, we examined the steady state photoluminescence (PL) of P3HT:PCBM thin films prepared on various HTLs. The peak fluorescence intensity of the sample prepared on PEG–SH-modified AuNP/GO nanocomposites was enhanced by approximately 55% (Fig. 5). Because the resonance peak of the nanocomposite exhibited significant overlapping with the absorption spectrum of P3HT, we infer that the enhanced PL probably resulted from an increased degree of photon absorption due to the near-field effect. Local enhancement of the electromagnetic field surrounding the AuNPs can assist with energy dissipation, thereby increasing the number of excitons.[15] On the other hand, the scattering cross-section of the AuNP/GO nanocomposites was much lower in the wavelength range corresponding to the PL spectrum of P3HT. Therefore, the far-field effect should contribute less to the photocurrent enhancement.

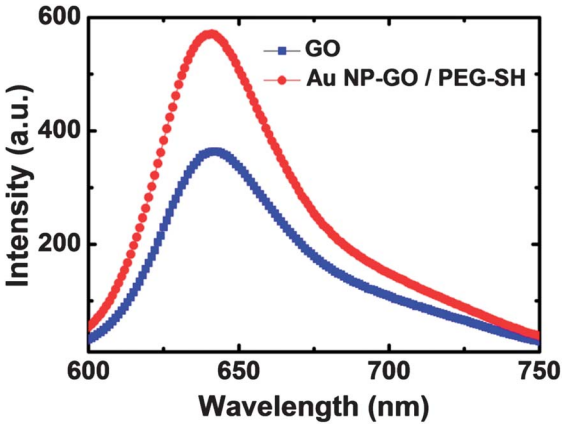

Fig. 5 PL spectra of P3HT thin films prepared on GO and AuNP/GO substrates.

Conclusions

In conclusion, we have synthesized AuNP/GO nanocomposites that improve the efficiency of OPVs by triggering LSPR. The AuNP/GO nanocomposites prepared with a weak capping agent possessed aggregated AuNPs on the GO surface. In contrast, the use of a stronger capping molecule, PEG–SH, prevented aggregation of the AuNPs and improved the solubility. When these nanomaterials served as the HTL, they introduced LSPR effects in the OPVs, leading to noticeable enhancements in the photocurrent and the efficiencies of the OPV devices under illumination at 1 sun. We attribute the primary origin of the improvement in device performance to local field enhancement induced by the LSPR. We anticipate that this study might open up new avenues for constructing plasmon-enhancing layers on the nanoscale to improve the performance of solar cells.

Experimental section

Synthesis of AuNP/GO composites

GO solutions were purchased from UniRegion Bio-Tech. The AuNP/GO composites were synthesized following the procedures reported in the literature.[30,31] First, an aqueous solution of GO (0.275 mg mL^{-1}, 3 mL) was added to a solution of $HAuCl_4$ (0.047 mg mL^{-1}, 10 mL) and then the mixture was aged for 30 min to

promote the interaction of the gold ions with the GO surfaces. The solution was heated at 80 °C before a solution of sodium citrate (0.085 mol dm^{-3}, 188 μL), a reducing agent, was added. The mixture was kept at 80 °C with continuous stirring for 4 h. Next, the solution was cooled to room temperature; while cooling, PEG–SH (molecular weight: 294.1 g mol^{-1}) was blended into the solution to modify the surface of the AuNPs. After stirring for 1 h, the resulting solution was centrifuged (6000 rpm) and washed three times with DI water to remove any free gold ions. Finally, the nanocomposites were dried through lyophilization.

Characterization

Absorption spectra were measured using an UV-Vis-near-IR spectrometer (PerkinElmer Lambda 950). Raman spectra were acquired on a Horoba high-resolution confocal Raman microscope equipped with a HeNe (632.8 nm) laser as the light source. PL spectra were obtained using an Ocean Optics spectrometer; a 532 nm laser was used as the excitation light source.

Device fabrication and testing

OPV devices were fabricated on patterned indium tin oxide (ITO)-coated glass substrates. The ITO-coated glass was treated with UV ozone prior to use. The GO and/or AuNP/GO compositions were then spin-coated onto the ITO substrates and then the samples were baked at 180 °C for 20 min. To improve the film quality, a mixed solvent system—H_2O and MeOH (1 : 2, v/v)—was adopted to dissolve the GO materials. The photoactive layer, prepared from a blend of P3HT and PCBM (1 : 1, w/w) in 1,2-dichlorobenzene, was spin-coated onto the GOs or AuNP/GO layer. [Devices were also prepared in which the acceptor (PCBM) was replaced by another C_{60} derivative, ICBA, which possesses a higher LUMO energy level,[36,37] to improve the open-circuit voltage.] The wet film underwent solvent annealing in a glass Petri dish for at least 20 min.[38,39] Prior to thermal evaporation of the cathode, consisting of Ca (30 nm) and Al (100 nm), the active blend was thermally annealed at 110 °C for 15 min. The *J–V* characteristics of the devices were measured using a Keithley 2400 source-measure unit. The photocurrent response was obtained under illumination from a 150 W Thermal Oriel solar simulator (AM 1.5G). The intensity of the light source was corrected using a standard Si photodiode.[40] The IPCE measurement system (Enli Technology) comprised a quartz tungsten halogen (QTH) lamp as the light source, a monochromator, an optical chopper, a lock-in amplifier, and a calibrated silicon photodetector.

Acknowledgements

We thank the National Science Council of Taiwan (Grant no. NSC 102-2221-E-009-130-MY3, NSC 102-3113-P-009-004, and NSC 101-2628-E-009-008-MY3) and the Ministry of Education of Taiwan (through the ATU program) for financial support.

References

1 L. M. Chen, Z. Hong, G. Li and Y. Yang, *Adv. Mater.*, 2009, **21**, 1434.
2 G. Dennler, M. C. Scharber and C. J. Brabec, *Adv. Mater.*, 2009, **13**, 1323.
3 H. L. Yip and A. K. Y. Jen, *Energy Environ. Sci.*, 2012, **5**, 5994.
4 J. D. Servaites, M. A. Ratner and T. J. Marks, *Energy Environ. Sci.*, 2011, **4**, 4410.
5 A. L. Roes, E. A. Alsema, K. Blok and M. K. Patel, *Prog. Photovoltaics*, 2009, **17**, 372.
6 G. Li, R. Zhu and Y. Yang, *Nat. Photonics*, 2012, **6**, 153.
7 S. H. Park, A. Roy, S. Beaupre, S. Cho, N. Coates, J. S. Moon, D. Moses, M. Leclerc, K. Lee and A. J. Heeger, *Nat. Photonics*, 2009, **3**, 297.
8 K. Tvingstedt, V. Andersson, F. Zhang and O. Inganas, *Appl. Phys. Lett.*, 2007, **91**, 123514.
9 Y. H. Zhou, F. L. Zhang, K. Tvingstedt, W. J. Tian and O. Inganas, *Appl. Phys. Lett.*, 2008, **93**, 033302.
10 J. Y. Kim, S. H. Kim, H. H. Lee, K. Lee, W. L. Ma, X. Gong and A. J. Heeger, *Adv. Mater.*, 2006, **18**, 572.
11 F. C. Chen, J. L. Wu and Y. Hung, *Appl. Phys. Lett.*, 2010, **96**, 193304.
12 Q. Gan, F. J. Bartoli and Z. H. Kafafi, *Adv. Mater.*, 2013, **25**, 2385.
13 D. H. Wang, J. H. Park, J. H. Seo, J. Seifter, J. H. Jeon, J. K. Kim, J. H. Park, O. O. Park and A. J. Heeger, *Adv. Energy Mater.*, 2011, **1**, 766.
14 X. Li, W. C. H. Choy, H. Lu, W. E. I. Sha and A. H. P. Ho, *Adv. Funct. Mater.*, 2013, **21**, 2728.
15 J. L. Wu, F. C. Chen, Y. S. Hsiao, F. C. Chien, P. Chen, C. H. Kuo, M. H. Huang and C. S. Hsu, *ACS Nano*, 2011, **5**, 959.
16 X. Yang, C. C. Chueh, C. Z. Li, H. L. Yip, P. Yin, H. Chen, W. C. Chen and A. K. Y. Jen, *Adv. Energy Mater.*, 2013, **3**, 666.
17 S. W. Baek, J. Noh, C. H. Lee, B. S. Kim, M. K. Seo and J. Y. Lee, *Sci. Rep.*, 2013, **3**, 1726.
18 G. Q. Fan, Q. Q. Zhou, J. J. Zhu, Z. Q. Xu, P. P. Cheng, Y. Q. Li, X. H. Sun, S. T. Lee and J. X. Tang, *J. Mater. Chem.*, 2012, **22**, 15614.
19 M. Jørengsen, K. Morrman and F. C. Krebs, *Sol. Energy Mater. Sol. Cells*, 2008, **92**, 686.
20 S. Park and R. S. Ruoff, *Nat. Nanotechnol.*, 2009, **4**, 217.
21 E. Morales-Narváez and A. Merkoçi, *Adv. Mater.*, 2012, **24**, 3298.
22 Y. Zhu, D. K. James and J. M. Tour, *Adv. Mater.*, 2012, **24**, 4924.
23 J. I. Paredes, S. Villar-Rodil, M. J. Fernández-Merino, L. Guardia, A. Martínez-Alonso and J. M. D. Tascón, *J. Mater. Chem.*, 2011, **21**, 298.
24 C. X. Guo, G. H. Guai and C. M. Li, *Adv. Energy Mater.*, 2011, **1**, 448.
25 S. S. Li, K. H. Tu, C. C. Lin, C. W. Chen and M. Chhowalla, *ACS Nano*, 2010, **4**, 3169.
26 J. M. Yun, J. S. Yeo, J. Kim, H. G. Jeong, D. Y. Kim, Y. J. Noh, S. S. Kim, B. C. Ku and S. I. Na, *Adv. Mater.*, 2011, **23**, 4923.
27 V. C. Tung, J. Kim and J. Huang, *Adv. Energy Mater.*, 2012, **2**, 299.
28 J. Liu, Y. Xue, Y. Gao, D. Yu, M. Durstock and L. Dai, *Adv. Mater.*, 2012, **24**, 2228.
29 X. Liu, H. Kim and L. J. Guo, *Org. Electron.*, 2012, **14**, 591.

30 Z. Zhang, H. Chen, C. Xing, M. Guo, F. Xu, X. Wang, H. J. Gruber, B. Zhang and J. Tang, *Nano Res.*, 2011, **4**, 599.
31 E. Dervishi, S. Bourdo, J. A. Driver, F. Watanabe, A. R. Biris, A. Ghosh, B. Berry, V. Saini and A. S. Biris, *ACS Nano*, 2012, **6**, 501.
32 C. Tan, X. Huang and H. Zhang, *Mater. Today*, 2013, **16**, 29.
33 Z. Luo, Y. Lu, L. A. Somers and A. T. C. Johnson, *J. Am. Chem. Soc.*, 2009, **131**, 898.
34 A. Esfandiar, O. Akhavan and A. Irajizad, *J. Mater. Chem.*, 2011, **21**, 10907.
35 A. C. Ferrari and J. Robertson, *Phys. Rev. B: Condens. Matter Mater. Phys.*, 2000, **61**, 14095.
36 G. J. Zhao, Y. J. He and Y. F. Li, *Adv. Mater.*, 2010, **22**, 4355.
37 Y. J. He, H. Y. Chen, J. H. Hou and Y. F. Li, *J. Am. Chem. Soc.*, 2010, **132**, 1377.
38 G. Li, Y. Yao, H. Yang, V. Shrotriya, G. Yang and Y. Yang, *Adv. Funct. Mater.*, 2007, **17**, 1636.
39 F. C. Chen, C. J. Ko, J. L. Wu and W. C. Chen, *Sol. Energy Mater. Sol. Cells*, 2010, **94**, 2426.
40 V. Shrotriya, G. Li, Y. Yao, T. Moriarty, K. Emery and Y. Yang, *Adv. Funct. Mater.*, 2006, **16**, 2016.